Beyond radical-rebound: Methane oxidation to methanol catalyzed by iron species in metal–organic framework nodes

Matthew C. Simons,[a] Steven D. Prinslow,[b] Melike Babucci,[c] Adam S. Hoffman,[d] Jiyun Hong,[d] Jenny G. Vitillo,[e] Simon R. Bare,[d] Bruce C. Gates,[c] Connie C. Lu,[b] Laura Gagliardi,[f] Aditya Bhan*[a]

[a] Department of Chemical Engineering and Materials Science, University of Minnesota, 421 Washington Avenue SE, Minneapolis, Minnesota 55455, United States

[b] Department of Chemistry, Chemical Theory Center, and Supercomputing Institute, University of Minnesota, 207 Pleasant Street SE, Minneapolis, Minnesota 55455, United States

[c] Department of Chemical Engineering, University of California, Davis, California 95616, United States

[d] SSRL, SLAC National Accelerator Laboratory, Menlo Park, CA 94025, USA

[e] Department of Science and High Technology and INSTM, University of Insubria, 22100 Como, Italy

[f] Department of Chemistry, Pritzker School of Molecular Engineering, The James Franck Institute and Chicago Center for Theoretical Chemistry, The University of Chicago, Chicago, IL 60637, United States

ABSTRACT: Recent work has exploited the ability of metal-organic frameworks (MOFs) to isolate Fe sites that mimic the structures of sites in enzymes that catalyze selective oxidations at low temperatures, opening new pathways for the valorization of underutilized feedstocks such as methane. Questions remain as to whether the radical-rebound mechanism commonly invoked in enzymatic and homogeneous systems also applies in these rigid-framework materials, in which resisting the over-oxidation of desired products is a major challenge. We demonstrate that MOFs bearing Fe(II) sites within Fe_3-μ_3-oxo nodes are active for conversion of CH_4 + N_2O mixtures (at 368-408 K), requiring steps beyond the radical-rebound mechanism to protect the desired CH_3OH product. Infrared spectra and density functional theory show that $CH_3OH_{(g)}$ is stabilized as Fe(III)-OCH_3 groups on the MOF via hydrogen atom transfer with Fe(III)-OH groups, eliminating water. Consequently, upon addition of a protonic zeolite in inter- and intra-pellet mixtures with the MOF, we observed increases in CH_3OH selectivity with increasing zeolite:MOF ratios and proximity of zeolitic H^+ sites to MOF Fe(II) sites, as methanol is protected within the zeolite. We infer from the data that $CH_3OH_{(g)}$ is formed via the radical-rebound mechanism on Fe(II) sites and that subsequent transport and dehydration steps protect $CH_3OH_{(g)}$ from over-oxidation. The results demonstrate that the radical-rebound mechanism commonly invoked in this chemistry is insufficient to explain the reactivity of these solid catalysts and that the selectivity-controlling steps involve both chemical and physical rate phenomena. The results point to a potential strategy to mitigate over-oxidation in these and similar systems.

INTRODUCTION

Methane, the primary component of natural gas, has emerged as a transitional low-carbon-intensity feedstock as the world evolves from its dependence on crude oil and coal to carbon-free energy carriers. Methanol, a high-energy-density liquid fuel, is formed by partial oxidation of methane, but industrial catalytic processes based on this conversion are still lacking because the strong, apolar C–H bonds in methane present formidable kinetic bottlenecks. Further, because the C–H bonds in methane are stronger than those in methanol, methanol formed from methane is readily over-oxidized to CO_2.[1] *Selective* functionalization of C–H bonds occurs in enzymes, via complex electron-transfer and gating mechanisms involving reactive metal-oxo centers,[2,3] and consequently researchers have worked for decades on molecular analogues of these enzymes, establishing that the conversion of Fe(II) sites to highly reactive Fe(IV)=O species is one motif capable of activating and functionalizing C–H bonds.[4,5] In attempts to mimic the chemistry of these sites in porous, crystalline supports, researchers have shown that Fe(II) sites in particular ion-exchange positions within zeolites form highly reactive α-oxygen species capable of oxidizing methane.[6–10] Solomon and coworkers determined that the α-oxygen species is a mononuclear Fe(IV)=O species formed by reaction of N_2O with a strained, square-planar, mononuclear Fe(II) species.[11,12] CH_4 activation at ambient temperature was proposed to proceed by a radical-rebound mechanism favored by the strained geometry of the active site and the high spin state of the Fe species conferred by the weak ligand field provided by zeolite framework oxygen atoms.[11] Other work has implicated diiron sites for methane oxidation using H_2O_2 as the terminal oxidant,[13] with secondary Cu sites working to prevent sequential oxidation pathways. Recently, these concepts have been extended[14,15] to another class of crystalline, porous materials, metal organic frameworks,[16–18] that proffer a distinct advantage over zeolite formulations by affixing active iron species in well-defined framework positions within an ultra-high surface area and thermally and chemically stable material. Initial postulates emerging from a

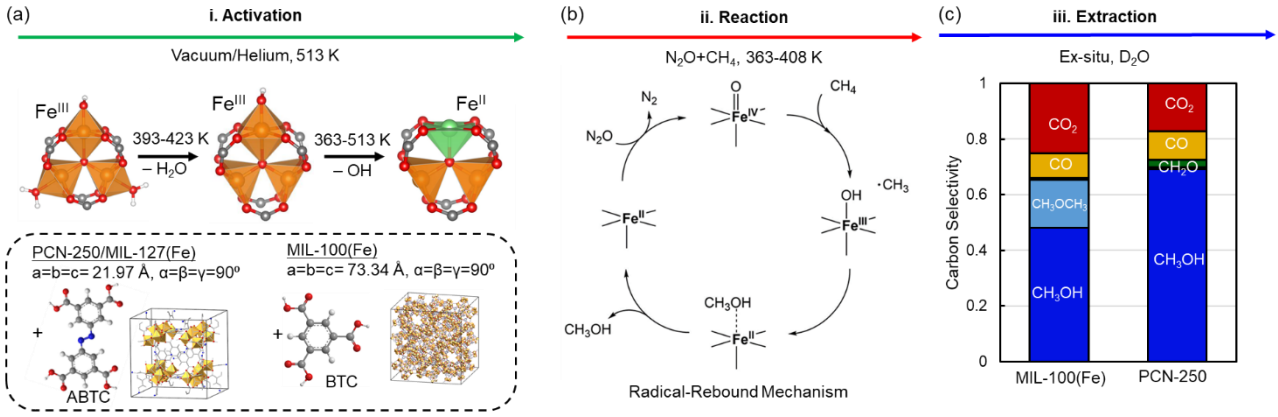

Figure 1. Depiction of the stepped reaction scheme employed in methane activation by Fe_3-μ_3-oxo-containing MOFs. (a) Molecular structure of the Fe_3-μ_3-oxo secondary building unit and depiction of how ligand occupancy changes upon thermal activation. Inset: Unit cells of PCN-250 and MIL-100(Fe) with the corresponding linkers (ABTC = 3,3′,5,5′-azobenzenetetracarboxylate, BTC = benzene-1,3,5-tricarboxylate). (b) Schematic representation of how the radical-rebound mechanism is proposed to activate methane on mononuclear Fe(II) centers exposed to mixtures of N_2O + CH_4.[19] (c) Cumulative carbon selectivity of products observed upon exposure of MIL-100(Fe) (60 mg)/PCN-250 (27 mg) to 80 kPa N_2O, 10 kPa CH_4, and 10 kPa Ar at 393 K for 4 h and quantified on-line (for CO ,CO_2) and *ex-situ* (for CH_3OH, CH_3OCH_3, CH_2O). Product selectivity (ascending order): CH_3OH (dark blue), CH_3OCH_3 (light-blue), CH_2O (green), CO (yellow), CO_2 (red).

computational study[19] that indicate isolated Fe(II) centers in Fe_3-μ_3-oxo nodes, common building units in an expansive family of MOFs,[20] in a weak ligand field imparted by carboxylate linker molecules, can form Fe(IV)=O moieties effective for subsequent C-H activation have been verified by Simons et al.[21] using a combination of Mössbauer and X-ray absorption spectroscopies and chemical titrations.

Reports characterizing these[19] and other Fe-containing MOFs[15,22,23] and zeolites[11] consistently invoke the radical rebound mechanism ascribed to homogeneous and enzymatic catalysts,[24–26] or lack mechanistic hypotheses. Open questions pertain to the catalytic nature of Fe(II) sites that could facilitate the formation of vapor-phase CH_3OH in these materials, and to mechanisms that protect the kinetically vulnerable methanol product. We now present evidence that MOF-supported systems containing similar Fe(II) sites form stabilized methoxy groups in reactions that form gaseous methanol, formed via the radical rebound mechanism, with Fe(III)-OH groups that are formed *in-situ*. Pursuant to this understanding, we offer a potential strategy for resisting over-oxidation using bifunctional, physical mixtures of H^+ form zeolites with Fe(II)-containing MOFs.

We first disclose herein the MOF platform, PCN-250,[20] containing Fe(II) sites situated in Fe_3-μ_3-oxo nodes, and show that it activates methane at temperatures < 398 K via a stepped reaction scheme. Methanol that remains adsorbed within the material after exposure to CH_4 and the oxidant N_2O and has been quantified *ex-situ* with ^{1}H-NMR spectroscopy. We evince, using *in-situ* infrared (IR) spectroscopy, that methanol is stabilized as Fe(III)-OCH_3 groups on the MOF via reactions with Fe(III)-OH moieties formed *in-situ*. Pursuant to this, we prepared a composite catalyst by adding a zeolite (MFI, Si/Al = 11.5) in inter- and intra-pellet mixtures with the MOF, and observe a monotonic increase in methanol selectivity with increasing zeolite: MOF ratio and proximity of zeolitic H^+ (H^+_{MFI}) to MOF Fe(II) sites ($Fe(II)_{MOF}$). We ascribe this trend to a molecular entity stable in the vapor phase, likely methanol, which can diffuse out of the MOF particles to be dehydrated and protected within the zeolite particles. These observations show, for the first time, that gaseous methanol is a product of methane activation on supported Fe sites, providing vital evidence for the applicability of the radical-rebound mechanism on Fe sites supported in solid catalysts—while also demonstrating that this mechanism is insufficient to fully explain the reactivity of these systems. Further, the data demonstrate that incorporation of nearby catalyst particles with a complementary function to capture and protect methanol affords a potential strategy to mitigate over-oxidation of methane and potentially other reactants with strong C–H bonds.

RESULTS AND DISCUSSION

Following our report documenting the ability of high-spin (S = 2) Fe(II) sites in MIL-100(Fe) to activate C_3H_8,[21] via a Fe(IV)=O intermediate formed by reaction of these sites with N_2O, Hall and Bollini[27] reported the stoichiometric formation of methanol from CH_4 + N_2O mixtures on these sites in MIL-100(Fe). This MOF contains Fe_3-μ_3-oxo nodes (Figure 1a) that incorporate a maximum of one Fe(II) site per node, and these are connected by benzene-1,3,5-tricarboxylate linkers (Figure 1a, inset).

In the work reported here, we address the reactivity of this common Fe(II) site in MIL-100(Fe) by comparison with PCN-250 (Figure 1a, inset), a MOF that is formed with 3,3′,5,5′-azobenzenetetracarboxylate linkers, before seeking to provide details of the function of these materials as it relates to the production and stabilization of the desired methanol product. Details of our experimental and computational methods are presented in Section S1 of the supplementary information.

Structure and reactivity of PCN-250. The common Fe_3-μ_3-oxo secondary building unit, synthesizable as $Fe_3(\mu_3\text{-}O)$ acetate clusters, in PCN-250 and in MIL-100(Fe) (Figure 1a) that hosts the Fe(II) site implies that each material should be able to activate methane using N_2O as an oxidant. The as-synthesized Fe_3-μ_3-oxo clusters do not show any reactivity as non porous agglomerates, but situated as separate nodes within MOF frameworks they display reactivity in a stepped

reaction scheme that involves sequential (i) activation of the material in an *in-vacuo* thermal treatment at high temperatures to form Fe(II) centers (Figure 1a), (ii) contact of the activated material with mixtures of N_2O + CH_4 to induce C–H bond scission (Figure 1b), and (iii) *ex-situ* extraction of methanol products with D_2O (Figure 1c). Herein we provide evidence for the structure and reactivity of the MOF PCN-250 that heretofore has not been investigated for reactions with N_2O + CH_4, demonstrating key similarities to MIL-100(Fe), and some differences too.

PCN-250 was synthesized following literature reports,[20] with modifications made to the final workup procedure to fully desorb solvent molecules from the pores that were found to otherwise interfere with the reactivity. Bulk structural properties were confirmed by X-ray diffraction (XRD) crystallography (Figure S1) and N_2 adsorption measurements (Figure S2-S3), confirming the expected single-phase crystallinity and porosity of the material. The formation of high-spin (S = 2) Fe(II) centers upon thermal treatment was confirmed *ex-situ* with Mössbauer spectroscopy (Figure S4), with the data indicating that approximately 27% of the Fe species (Table S1) were reduced from Fe(III) to Fe(II); the corresponding value for the sample of MIL-100(Fe) used in these experiments was 18% (Figure S5, Table S2). NO was used as a chemical titrant for unsaturated Fe(II) sites to supplement these results.[28,29] IR spectra of PCN-250 recorded during dosing of increasing amounts of NO gas (Figure S6) yield absorption bands in the range of 1788-1804 cm^{-1}, consistent with Fe(II)-NO adducts determined experimentally[28] or computed with DFT.[29] Thus, the data demonstrate the formation of coordinatively unsaturated Fe(II) centers upon thermal activation. The loss of H_2O molecules and -OH moieties (Figure 1a) to form open metal centers was observed explicitly as broad absorption bands (2400-3600 cm^{-1}), signifying H_2O agglomerates, and a $\nu_{O\text{-}H}$ band at 3682 cm^{-1}, assigned to a Fe(III)-OH group (*vide infra*), disappeared during activation as the temperature was increased to 523 K (Figure S7).

In-situ X-ray absorption spectroscopy was used to provide further evidence of changes in the oxidation state and coordination of Fe, both after the thermal activation and after reaction with N_2O + CH_4. Shifts of the absorption edge energy to lower values in the X-ray absorption near edge structure (XANES) data after thermal activation in helium to 513 K were accompanied by a decrease in white-line intensity and an increase in the pre-edge peak intensity (Figure 2a). The edge energy is one indicator of the iron formal oxidation state,[30] and it has been used previously to quantify the interconversion of Fe(III) centers to Fe(II) in MIL-100(Fe).[21] Comparing the edge energy of PCN-250 with those of reference compounds (Figure S8-S10), we infer from XANES that thermal activation converts 18–22% of the Fe(III) sites to Fe(II) sites (Figure S11 and S12 in the SI), in agreement with *ex-situ* Mössbauer spectra (*vide supra*). The magnitude of the Fourier transform (FT) of the EXAFS spectrum at 2.03 Å (Figure 2b) also decreased slightly. After reaction with N_2O + CH_4 at 393 K, the absorption edge position had shifted back to a higher value, and the magnitude of the FT at 2.04 Å had increased, indicating that Fe(II) sites were consumed and converted back to Fe(III).[30–32] Isosbestic points in the Fe K edge XANES spectra acquired during

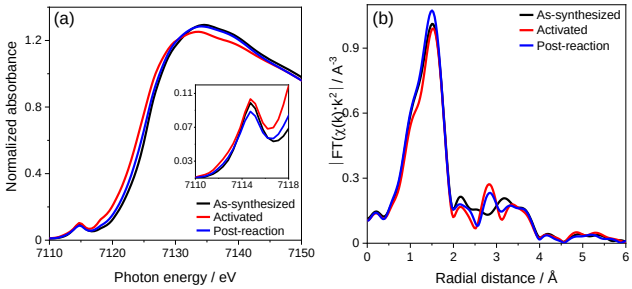

Figure 2. (a) Fe K-edge XANES, with inset showing the pre-edge peaks, and (b) EXAFS data (magnitude of the Fourier transform (k^2-weighted)) characterizing PCN-250 after various treatments: in flowing helium at 393 K and then at 513 K; and after reaction with N_2O + CH_4 at 393 K.

treatment and reaction with N_2O + CH_4 (Figure S8 in the SI) indicate that the changes in the structure of the Fe species were stoichiometrically simple.

Structural models of the Fe sites inferred from the EXAFS data (Table S3-S4, Figures 2b, S13–S28) characterizing the as-synthesized PCN-250 are consistent with the known structure of PCN-250 determined by XRD crytallography.[20] Activation at temperatures from 398–513 K led to a negligible change in the average Fe–O coordination number, from 5.8 ± 0.5 to 5.6 ± 0.5 (Figure 2b, Table S4), consistent with axial -OH ligands being removed in the reduction of Fe(III) centers to open Fe(II) sites (Figure 1a). After reaction with N_2O + CH_4 at 393 K, the average Fe–O coordination number had increased again, suggesting that the Fe species in the nodes were again coordinated to axial ligands in the positions where they had been originally.

XANES, EXAFS, and Mössbauer data show that thermal activation induces changes in the coordination and oxidation state of Fe in PCN-250, forming Fe sites that are similar to Fe centers in αKG-dependent dioxygenases in geometry and spin-state.[21,26] Exposure to N_2O + CH_4 mixtures at 363–393 K in a recirculating batch reactor led to conversion of these species accompanied by the formation of gas-phase CO and CO_2. CH_3OH and other products (CH_3OCH_3, CH_2O) remained adsorbed within the MOF, and are observed only after the material was washed with D_2O *ex-situ* and quantified with ^1H NMR spectroscopy (Figure 1c). These results confirm recent work[19,27] demonstrating that the putative Fe(IV)=O species oxidizes CH_4 to methanol and other products (CH_3OCH_3, CH_2O, CO, CO_2). A key difference between the two MOFs is in product selectivity, with MIL-100(Fe) having a higher selectivity for CH_3OCH_3 than PCN-250, seemingly at the expense of CH_3OH. We posit the role of secondary species linked to the defective nature of the MIL-100(Fe) sample (18% Fe(II) concentration compared with the 33% if every Fe_3-μ_3-oxo node is active) in effecting the formation of CH_3OCH_3 from CH_3OH in additional steps. The existence of distinct secondary pathways converting CH_3OH to CH_3OCH_3 is supported by experiments discussed in the next section, whereby capturing gaseous methanol with a protonic ZSM-5 zeolite decreases the selectivity to CH_3OCH_3 in MIL-100(Fe) systems.

Batch reactor experiments with varied N_2O partial pressures show that the N_2 formation and CH_4 consumption reactions are first order in N_2O (Figure S29) but almost zero order in CH_4 (Figure S30), congruent with the postulate of

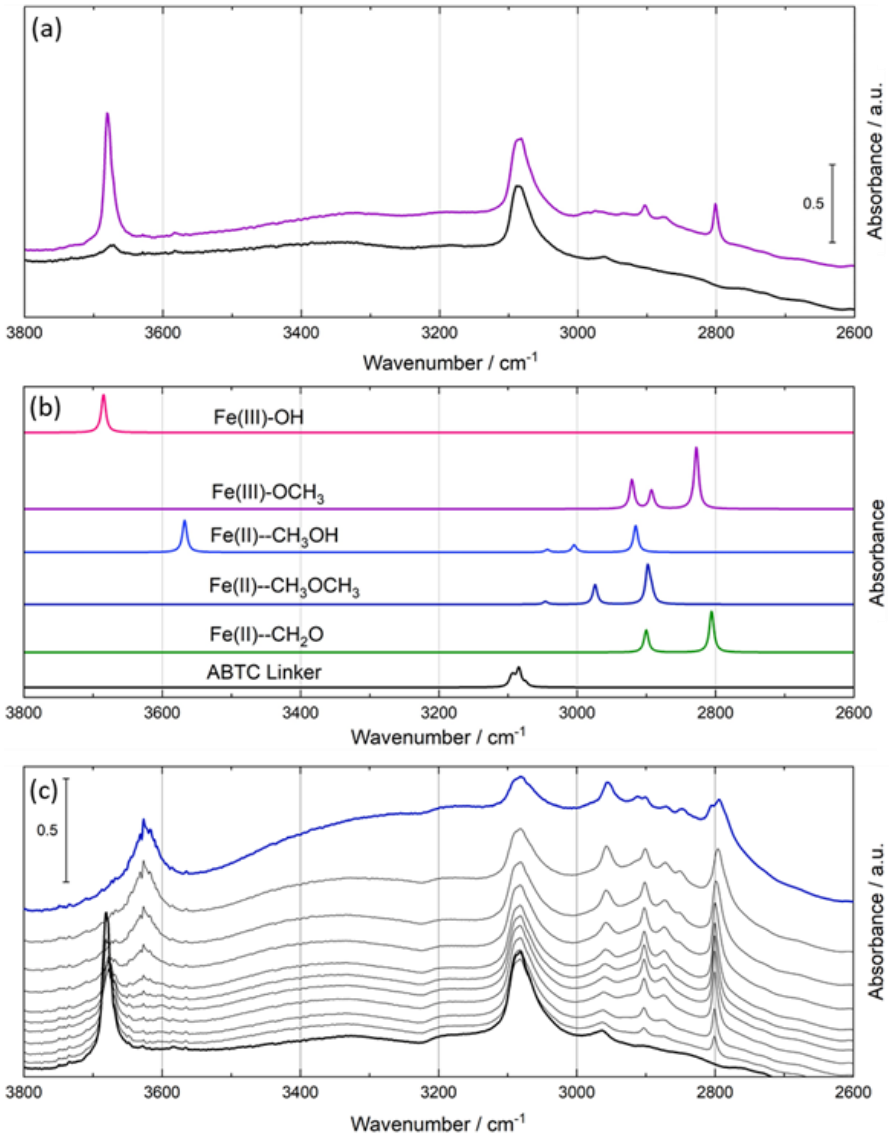

Figure 3. a) IR spectra of PCN-250 (20mg) treated to 513 K *in-vacuo* before (black) and after (purple) exposure to a 4:1 flow of N_2O and CH_4 at 393 K for 4h. b) DFT computed vibrational frequencies of different surface species modelled on a single Fe_3-μ_3-oxo cluster (top to bottom: -OH, -OCH_3, CH_3OH, CH_3OCH_3, CH_2O, ABTC linker). C) IR spectra of PCN-250 (20 mg, treated at temperatures up to 423 K *in- vacuo)* at 393 K (black) and with added increments (1–2 μmol each) of CH_3OH vapor (grey) until the pressure reached 450 Pa (blue).

an initial rate-limiting reaction of N_2O with the Fe(II) center to form a highly reactive Fe(IV)=O species, as was reported for the $N_2O + C_3H_8$ reaction on MIL-100(Fe).[21] The non-zero-order dependence of the initial rate of CH_4 conversion on CH_4 partial pressure suggests there are regimes in which CH_4 activation by an Fe(IV)=O group is kinetically significant for CH_4 consumption, although DFT calculations predict a substantially higher intrinsic barrier for Fe(IV)=O formation (95 kJ mol^{-1})[21] and CH_4 activation (60 kJ mol^{-1}).[19] The reactivity of PCN-250 and MIL-100(Fe) can be compared explicitly through measurements of Arrhenius activation energy barriers for N_2 production (Figure S31). Normalizing reaction rates by Fe(II) concentration collapses first order rate constants to within a factor of two for these materials, and varying temperatures results in similar values for activation energy barriers, 79.2 ± 7.6 kJ mol^{-1} and 79.1 ± 5.8 kJ mol^{-1}, for the reaction of N_2O with Fe(II) on PCN-250 and MIL-100(Fe), respectively, in quantitative agreement with the computed barrier (85 kJ mol^{-1}) for N_2O activation on a single cluster model of the Fe_3-μ_3-oxo nodes.[19,21] Recycle experiments using the same sample of PCN-250 showed no significant changes in product yield or selectivity (Figure S32).

Mechanisms of CH_3OH formation and stabilization. Activation of methane to form methanol on this Fe(II) site is proposed, on the basis of DFT calculations,[19,21] to occur via a radical-rebound mechanism, consistent with the proposed mechanism for C–H bond hydroxylation in enzymatic, homogeneous, and supported catalysts incorporating metal-oxo sites. Nonetheless, reactions of N_2O + CH_4 on PCN-250 and MIL-100(Fe) are characterized by significant selectivity to various over-oxidation products (CH_2O, CO, CO_2) and other products (CH_3OCH_3). These observations are unsurprising as further CH_3OH oxidation is both kinetically and thermodynamically favored (Figure S33), with the maximum yield of methanol formed determined by the relative

susceptibilities of methanol and methane to be oxidized (Figure S34).[1] The C–H bond scission step is not readily accessible to experimental investigation, but DFT calculations (Section S6) show that methanol reacts so readily with Fe(IV)=O that experimental determination of the CH_3OH yield is expected to be extremely difficult. But experimentally methanol is observed as the major product after washing the material *ex-situ*; gaseous methanol, predicted to be formed by the commonly invoked radical-rebound mechanism, was not observed, consistent with observations made with other supported Fe-containing solids.[9,10,27,33,34] We thus posited that in binding methanol to the MOF, deleterious over-oxidation pathways are minimized, motivating us to investigate the mechanism of CH_3OH protection.

We sought to identify the adsorbed methanol species under reaction conditions using *in-situ* IR spectroscopy. Spectra of PCN-250 (Figure 3a) activated by heating to 513 K *in vacuo* show the exclusive presence of ν_{CH} bands belonging to the ABTC linker (3082–3076 cm^{-1})—consistent with the removal of solvent molecules and axial ligands leading to the formation of open Fe(II)/Fe(III) sites (Figure 1a).[21,35,36] After exposure of the activated sample to N_2O + CH_4 at 393 K, we observed the appearance of two sets of bands: ν_{CH} bands at 2904, 2876, and 2802 cm^{-1} and a ν_{OH} band at 3682 cm^{-1}. The three ν_{CH} bands correlate with methanol formation quantified with ^{1}H-NMR spectroscopy data determined after washing the IR wafer with D_2O (Figure S35-36), thus allowing us to assign these bands to specific C–H vibrational modes of a stabilized methanol-derived species.[37] DFT calculations were used to aid the assignment of these bands by considering candidate adsorbed species on a single-cluster model of the Fe_3-μ_3-oxo nodes of PCN-250 and MIL-100(Fe) (Figure S40). Similar models have been used to accurately predict the apparent energy barriers for the rate limiting N_2O + Fe(II) reaction step,[19,21,38] and a similar cluster model and level of theory (see Sections S1 and S9.1 for full details of computations) have been used to accurately assign IR bands to surface groups on the Zr-containing MOF NU-1000,[39] scaling the computed vibrational frequencies by a factor of 0.958 to ensure appropriate comparison with experiment.[40] The closest agreement between the models considered (Figure 3b, Section S9.1) and experimental observations is achieved with a methoxy group affixed to one Fe atom on the Fe_3-μ_3-oxo node (Fe(III)–OCH_3,). Each computed band is shifted by 20–25 cm^{-1} to higher wavenumbers relative to experiment, within the expected error for computations at this level of theory.[39,40]

In contrast, calculations for physisorbed methanol predict vibrational bands at much higher wavenumbers, confirmed experimentally by dosing gaseous methanol onto PCN-250 (Figure S37) and the observation of ν_{CH} bands at 2846 and 2958 cm^{-1}, a ν_{OH} band at 3620 cm^{-1}, and a broad absorption between 3200–3500 cm^{-1} assigned to hydrogen-bonded agglomerates of CH_3OH molecules, altogether allowing us to exclude these species. Assignment of this stable species formed *in situ* is consistent with the lack of a ν_{CO} stretching band at 1000–1020 cm^{-1}, which was evident in both experimental and DFT models of physisorbed methanol (Figure S38). These results allow us to rule out the dissociative adsorption of methanol on the bare Fe_3-μ_3-oxo nodes to form covalently bound, and thus stabilized, surface species, suggesting that an alternative mechanism is needed to protect the desired methanol product.

DFT calculations also led us to assign the ν_{OH} band observed *in situ* (3682 cm^{-1}) to Fe(III)-OH groups in the MOF nodes (Figure 3a-b). This group is a ligand present in the as-synthesized MOF and removed during activation in the autoreduction of Fe(III) species to form Fe(II) sites (Figure 1a), consistent with the EXAFS results (*vide supra*), but nonetheless it appears to form again *in situ*. Assignment of both sets of bands to methoxy and hydroxyl groups on molecular Fe sites is consistent with assignments made for similar Fe-exchanged ZSM-5 zeolite materials.[33,34]

The formation of this stable methoxy group from the reaction of CH_4 + N_2O with the Fe(II) centers opens a route to the production of methanol in high selectivity—provided that a separate step is invoked to extract this species without over-oxidizing it—such over-oxidation is broadly characteristic of selective oxidation on other metal-oxo species on solid supports.[10,33,41] Significantly, the formation of this methoxy group is not consistent with the radical-rebound mechanism (Figure 1b), which predicts the formation of gaseous methanol only. We consequently hypothesize that the methoxy species forms as CH_3OH molecules react with surface hydroxyl groups (ν_{OH} = 3682 cm^{-1}) observed *in situ*, eliminating H_2O. This pathway offers a potential route for the protection of gaseous methanol, otherwise unobserved but predicted by DFT calculations to be produced by the radical-rebound mechanism.[19]

We proffer evidence for the plausibility of this reaction pathway first with IR spectroscopy. PCN-250 was heated *in-vacuo* to 413 K, an intermediate temperature that removes physisorbed solvent molecules but not nascent Fe(III)-OH groups present in the as-synthesized MOF (Figure 3c, black). Then a small dose (0.05–1 μmol per mg of PCN-250) of gas-phase CH_3OH ($CH_3OH_{(g)}$) was added (Figure 3c, gray) at 393 K, leading to an immediate decrease in intensity of the ν_{OH} band and formation of the three ν_{CH} bands (2904, 2876, and 2802 cm^{-1}) assigned to an Fe(III)-OCH_3 moiety. This result provides evidence that Fe(III)-OH groups react with CH_3OH at low (<40 Pa) partial pressures at the reaction temperature (393 K) to form the stabilized Fe(III)-OCH_3 species we observed *in situ* and resulting from the reaction of N_2O + CH_4 on PCN-250. These changes continued upon further incremental addition of $CH_3OH_{(g)}$ until the ν_{OH} band was mostly consumed, at which point bands attributable to methanol physisorbed on the MOF (Figure S39) became apparent.

DFT calculations were subsequently used to confirm the ability of this Fe(III)-OH group to eliminate H_2O and stabilize CH_3OH, signifiantly indicating that the mechanism in PCN-250 is different than the one reported for acidic supports, such as zeolites[42–45] and polyoxometalates.[46] In zeolites, single-step[44,45] and two step dehydration mechanisms[42] have been proposed that occur through concurrent or sequential protonation of methanol by the acid and subsequent C-O scission. A similar mechanism in PCN-250 would require the concerted (Figure 4a) or sequential (Figure S42) activation of the CH_3–OH and FeO–H bonds with the formation of the CH_3–OFe bond. The activation enthalpy reported for zeolites was found to be dependent on the system (ranging from 180–230 kJ mol^{-1} in SAPO-5, -11, -34, and

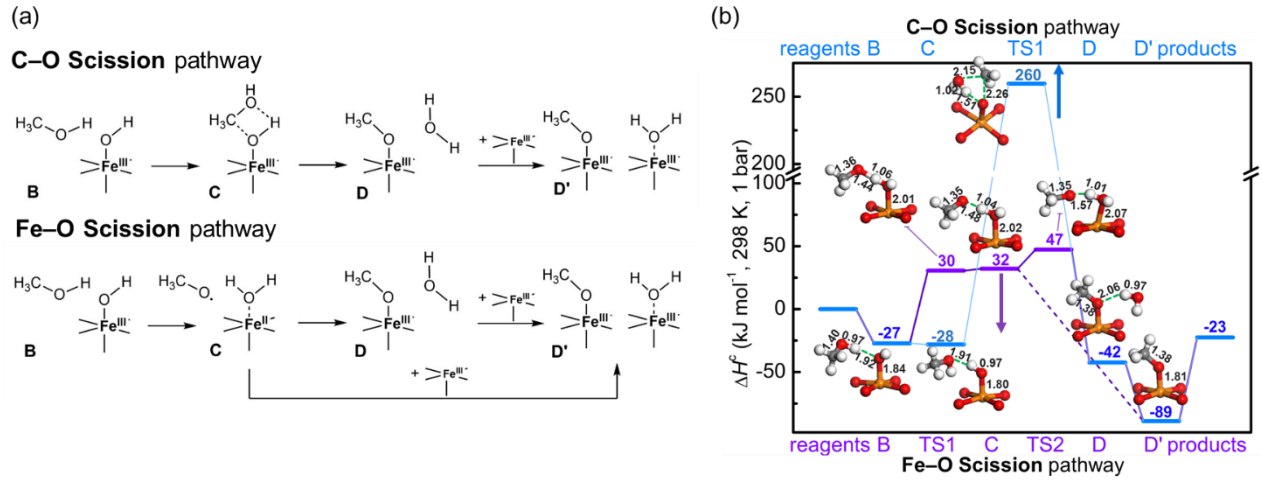

Figure 4. Methoxy formation from methanol over Fe(III)-OH sites PCN-250**. a)**. Schematics for methanol dehydration via C–O and Fe–O scission pathways. **b)**. Reaction enthalpy profiles for C–O (blue) and Fe–O (violet) scission dehydration pathways calculated at the UM06-L/def2-TZVP level on the 2S + 1 = 16 spin surface. The enthalpy of the separated reactants (the Fe_3-μ_3-oxo cluster and one methanol molecule) set the zero enthalpy. The optimized structure of the Fe center, its first coordination sphere, and interacting species is shown for each step. Color code: red (oxygen), grey (carbon), orange (iron), white (hydrogen).

-41 materials[44] to 90 kJ mol^{-1} in ZSM-5[45] in a concerted mechanism, and 80 kJ mol^{-1} in the two- step mechanism in ZSM-22[42]). Computing the reaction profiles of both single and two-step mechanisms via C-O scission (blue line in Figure 4a and Figure S42, respectively), using a Fe_3-μ_3-oxo cluster model previously employed,[19,21,38] predicts activation enthalpies of 288 and 181 kJ mol^{-1}, respectively. These values are unfeasible regarding experiments showing methoxy formation at 393 K (Figure 3). Instead, the surface hydroxyl group could act to abstract an H atom from methanol to form water, and proceed via Fe-O scission (Figure 4a) through displacement of the nascent H_2O molecule by a $CH_3O\cdot$ species (solid violet line, Figure 4b) or by the methoxy group attaching to an adjacent Fe site on the node (dashed violet line in Figure 4b). Intrinsic activation enthalpies of 57 and 74 kJ mol^{-1} for methoxy formation via Fe-O scission are compatible with experimental results, *vide supra*, suggesting that CH_3OH formally acts to dehydrate Fe(III)-OH groups, rather than the converse, on these Fe_3-μ_3-oxo MOFs to form a stabilized methoxy species.

A conceivable alternative pathway to produce Fe–OCH_3 groups would be that in which CH_3 radicals produced after the initial C–H bond scission event in the radical rebound mechanism do not rebound to the nascent Fe-OH group (Figure 1b). Instead, they would diffuse and attach to another Fe(IV)=O active center. There is evidence of alkyl radicals produced by C–H scission dissociating from active centers in homogeneous metal-oxo complexes,[47] and this reaction is almost barrierless (Figure S43). However, we infer that this route is unlikely to be relevant because of the low concentration of Fe(IV)=O groups; the reaction kinetics indicate a rate-limiting reaction of N_2O with Fe(II) sites to form Fe(IV)=O intermediates, which are then quickly consumed in the subsequent C–H scission step.

We sought further evidence that mechanistic steps that lie beyond the radical-rebound mechanism function to protect methanol from over-oxidation, in particular for (i) the formation of gaseous methanol from Fe(II) sites situated in the MOF and (ii) the ability of methanol produced within the MOF to diffuse from active Fe centers and undergo dehydration on nearby sites. We chose to probe these questions by adding a second material, a protonic zeolite (ZSM-5/MFI, Si/Al = 11.5), in physical mixtures with particles of PCN-250 or MIL-100(Fe), to give evidence of the ability of gaseous methanol, if present, to diffuse from Fe(II) centers within the MOF crystallites to zeolites and therein to undergo dehydration on the strong Brønsted acid sites therein.[45]

In interpellet mixtures, holding the amount of PCN-250 (24 μmol $Fe(II)_{MOF}$) and all other process parameters constant bar the amount of zeolite added to the fixed bed, we observed that the selectivity for methanol formation increased monotonically with increasing ratio of zeolite to MOF (Figure 5a). Constant values of the cumulative N_2 yield, a measure of the total number Fe(IV)=O groups created during reaction, across different physical mixtures confirm that adding a second functional material to the catalyst bed had no effect on the initial and rate-limiting reaction between Fe(II) sites and N_2O within the MOF particles. This result demonstrates that the increase in methanol selectivity observed upon addition of the zeolite is reflective of an improved ability of these multifunctional formulations to protect methanol from over-oxidation, as fewer Fe(IV)=O equivalents were consumed in over-oxidation reactions.

We confirmed that methanol was transported to zeolite particles by conducting equivalent experiments with interpellet mixtures incorporating MOF and zeolite particles of various sizes, separating them prior to *ex-situ* extraction to show that methanol (and CH_3OCH_3) were released from the zeolite particles (Figure S44). Control experiments carried out with N_2O + CH_4 mixtures in the presence of the zeolite without the MOF showed no activity, and no C_1 oxygenate products were observed *ex situ*.

Next, we tested the effect of increasing proximity of $Fe(II)_{MOF}$ sites to H^+_{MFI} sites through the use of inter- and intrapellet mixtures at fixed ratios of MOF to zeolite (Figure 5b), wherein intrapellet mixtures are formed from a physical mixture of the MOF and zeolite powders as a means to decrease the average $Fe(II)_{MOF}$:H^+_{MFI} distance. This results in

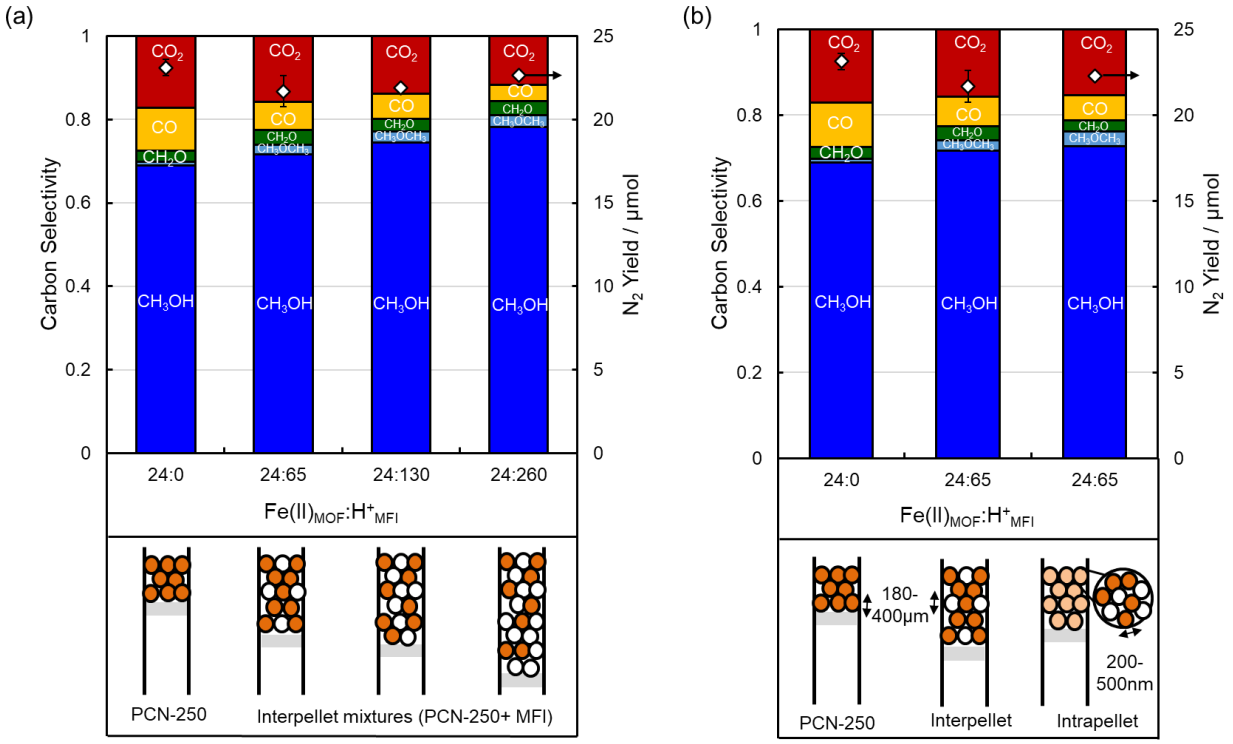

Figure 5. (a) Cumulative product selectivity (left ordinate) and N_2 yield (right ordinate) for interpellet physical mixtures of PCN-250 and MFI (Si/Al = 11.5). (b) Cumulative product selectivity (left ordinate) and N_2 yield (right ordinate) for intra- and inter- pellet physical mixtures of PCN-250 and MFI (Si/Al = 11.5). Reaction conditions: 393 K, 80 kPa N_2O, 10 kPa CH_4, 10 kPa Ar, 4 h reaction time, 27-29mg PCN-250 and 0-200mg MFI (Si/Al = 11.5) in the form of separate or mixed catalyst pellets (180-400 μm). Products given in ascending order: CH_3OH (blue), CH_3OCH_3 (sky-blue), CH_2O (green), CO (yellow), CO_2 (red), N_2 (open diamonds, error bars equal ± 2×Std.Dev.). Inset: Schematic showing configuration of the MOF and zeolite in the fixed bed reactor.

a further small increase in the yield (Figure S45-S46) and selectivity to methanol (71 to 73%) and DME (2.4 to 3.4%) (Figure 5b). The consequences of this are twofold. First, the increase in yield to methanol with closer proximity between Fe(II) centers and H^+ sites intimates the influence of diffusion within catalyst pores and between particles on reaction rates and therefore selectivity as more methanol is protected. Consistent with this conclusion, the increase in DME selectivity that becomes apparent upon addition and proximity of H^+_{MFI} demonstrate the ability of these bifunctional formulations to enhance secondary pathways. Equivalent experiments with physical mixtures of MIL-100(Fe) and ZSM-5 zeolite wherein the same trends with increasing ratio and proximity of $Fe(II)_{MOF}$ to H^+_{MFI} hold (Figure S47). These results demonstrate the ability of $CH_3OH_{(g)}$ molecules, not otherwise observed experimentally, to dissociate from the MOF-supported Fe(II) sites, exit the MOF particles, and be transported to zeolitic H^+ sites where they presumably undergo dehydration, and are thus protected from overoxidation. Although physisorption of methanol, enhanced by H-bonding with protonic sites and the small pores of the zeolite, can be partially responsible for methanol protection, the increase in selectivity to CH_3OCH_3 observed when ZSM-5 was added to mixtures with PCN-250 (Figure 5) suggests that methanol dehydration pathways within the zeolite are active under our reaction conditions.

Taken together, these results open avenues of research whereby improved bifunctional formulations can be targeted to minimize or enhance undesired or desired secondary reaction pathways.

CONCLUSIONS

In the Fe_3-μ_3-oxo nodes of PCN-250 and MIL-100(Fe), Fe(II) centers that bear coordination and spin states similar to those found in enzymatic and homogeneous systems effect CH_4 activation with N_2O as the oxidant. Prior DFT calculations suggest this activation occurs via the commonly cited radical-rebound mechanism, whereby the Fe(II) site reacts with N_2O in the rate-limiting step to form an Fe(IV)=O species that in turn activates CH_4 homolytically, producing CH_3OH molecules that dissociate from the active center to close the catalytic cycle. Thermodynamic and kinetic factors that drive methanol to rapidly over-oxidize led us to propose, on the basis of *in-situ* IR spectroscopy and DFT calculations, that methanol is protected within the MOF under reaction conditions as a methoxy group affixed to the nodes, the formation of which cannot be explained by the radical-rebound mechanism.

We present for the first time a plausible formation pathway for this stabilized species, having used IR spectroscopy to show that Fe(III)–OH reacts stoichiometrically with $CH_3OH_{(g)}$ present in low, Pascal-level concentrations to form Fe(III)–OCH_3 groups at reaction temperatures. A novel formulation consisting of physical mixtures of Fe-containing MOFs with MFI zeolites incorporating Brønsted acid groups was found to increase the amount of methanol protected from over-oxidation, signalling that $CH_3OH_{(g)}$, otherwise unobserved, is indeed produced by reactions of N_2O + CH_4 on the MOF and supporting the proposal that the radical-rebound mechanism, commonly invoked for other systems

and supported by DFT results, is indeed active in these systems. Moreover, the results show that $CH_3OH_{(g)}$ produced in the MOF has the ability to diffuse from Fe(II) sites, out of the MOF particles, and to zeolitic Brønsted acid groups, where it is catalytically dehydrated and thereby protected. These observations unequivocally evince additional mechanistic steps beyond the radical-rebound mechanism that act to protect product CH_3OH. We envision that in these catalysts, gas-phase CH_3OH produced via the radical rebound mechanism dissociates from the active center, whereupon it migrates either to a Fe(IV)=O group and reacts to form one of a number of over-oxidation products (CH_2O, CO, CO_2) or, alternatively, migrates to a Fe(III)–OH species, where it undergoes hydrogen atom transfer and is protected. The effects of both the zeolite:MOF ratio and the proximity of H^+_{MFI} sites to $Fe(II)_{MOF}$ sites on the selectivity of methanol formation demonstrate that both chemical and physical rate processes govern selectivity, providing guidance for the design of new systems that should seek to improve efficacy of dehydration on a particular site as well as proximity of this site to the Fe(II) center. These results provide a potential strategy for protecting the methanol during methane oxidation, whereby the desired product is both thermodynamically and kinetically driven to over-oxidation.

ASSOCIATED CONTENT

Supporting Information. Detailed descriptions experimental and computational methods, including of synthesis protocols, materials characterization (XRD, N_2 Isotherms, X-ray absorption spectroscopy, Mössbauer spectroscopy, IR spectroscopy), reactivity experiments, and DFT calculations with supplementary results. A separate .zip folder containing xyz coordinates of computational models is also provided. This material is available free of charge via the Internet at http://pubs.acs.org.

AUTHOR INFORMATION

Corresponding Author

* abhan@umn.edu

ACKNOWLEDGMENTS

This work was supported by the Inorganometallic Catalyst Design Center, an Energy Frontier Research Center funded by the US Department of Energy (DOE), Office of Science, Basic Energy Sciences (BES) (DE-SC0012702). The authors acknowledge the Minnesota Supercomputing Institute (MSI) at the University of Minnesota for providing computational resources. Mössbauer spectroscopy was performed at the Institute for Rock Magnetism (IRM) at the University of Minnesota with the help of Peter Solheid. The IRM is a US National Multi-user Facility supported through the Instrumentation and Facilities program of the NSF, Earth Sciences Division, and by funding from the University of Minnesota. We acknowledge the Stanford Synchrotron Radiation Lightsource (SSRL) for access to beam time on Beamline 9-3. SSRL, SLAC National Accelerator Laboratory, is supported by DOE BES, under Contract No. DE-AC02-76SF00515, and the DOE BES-funded Consortium for Operando and Advanced Catalyst Characterization via Electronic Spectroscopy and Structure (Co-ACCESS) at SLAC National Accelerator Laboratory.

REFERENCES

(1) Labinger, J. A. Selective Alkane Oxidation: Hot and Cold Approaches to a Hot Problem. *J. Mol. Catal. A Chem.* **2004**, *220* (1), 27–35. https://doi.org/10.1016/j.molcata.2004.03.051.

(2) Wallar, B. J.; Lipscomb, J. D. Dioxygen Activation by Enzymes Containing Binuclear Non-Heme Iron Clusters. *Chem. Rev.* **1996**, *96* (7), 2625–2657. https://doi.org/10.1021/cr9500489.

(3) Dinh, K. T.; Sullivan, M. M.; Serna, P.; Meyer, R. J.; Dincă, M.; Román-Leshkov, Y. Viewpoint on the Partial Oxidation of Methane to Methanol Using Cu- and Fe-Exchanged Zeolites. *ACS Catal.* **2018**, *8* (9), 8306–8313. https://doi.org/10.1021/acscatal.8b01180.

(4) Que, L. The Road to Non-Heme Oxoferryls and Beyond. *Acc. Chem. Res.* **2007**, *40* (7), 493–500. https://doi.org/10.1021/ar700024g.

(5) Que, Jr., L.; Puri, M. The Amazing High-Valent Nonheme Iron-Oxo Landscape. *Bull. Japan Soc. Coord. Chem.* **2016**, *67*, 10–18. https://doi.org/10.4019/bjscc.67.10.

(6) Dubkov, K. A.; Sobolev, V. I.; Panov, G. I. Low-Temperature Oxidation of Methane to Methanol on FeZSM-5 Zeolite. *Kinet. Catal.* **1998**, *39* (1), 72–79.

(7) Panov, G. I.; Dubkov, K. A.; Starokon, E. V. Active Oxygen in Selective Oxidation Catalysis. *Catal. Today* **2006**, *117* (1), 148–155.

(8) Dubkov, K. A.; Sobolev, V. I.; Talsi, E. P.; Rodkin, M. A.; Watkins, N. H.; Shteinman, A. A.; Panov, G. I. Kinetic Isotope Effects and Mechanism of Biomimetic Oxidation of Methane and Benzene on FeZSM-5 Zeolite. *J. Mol. Catal. A Chem.* **1997**, *123* (2–3), 155–161. https://doi.org/10.1016/S1381-1169(97)00051-4.

(9) Parfenov, M. V.; Starokon, E. V.; Pirutko, L. V.; Panov, G. I. Quasicatalytic and Catalytic Oxidation of Methane to Methanol by Nitrous Oxide over FeZSM-5 Zeolite. *J. Catal.* **2014**, *318*, 14–21. https://doi.org/10.1016/j.jcat.2014.07.009.

(10) Starokon, E. V.; Parfenov, M. V.; Arzumanov, S. S.; Pirutko, L. V.; Stepanov, A. G.; Panov, G. I. Oxidation of Methane to Methanol on the Surface of FeZSM-5 Zeolite. *J. Catal.* **2013**, *300*, 47–54. https://doi.org/10.1016/j.jcat.2012.12.030.

(11) Snyder, B. E. R.; Vanelderen, P.; Bols, M. L.; Hallaert, S. D.; Böttger, L. H.; Ungur, L.; Pierloot, K.; Schoonheydt, R. A.; Sels, B. F.; Solomon, E. I. The Active Site of Low-Temperature Methane Hydroxylation in Iron-Containing Zeolites. *Nature* **2016**, *536* (7616), 317–321. https://doi.org/10.1038/nature19059.

(12) Snyder, B. E. R.; Böttger, L. H.; Bols, M. L.; Yan, J. J.; Rhoda, H. M.; Jacobs, A. B.; Hu, M. Y.; Zhao, J.; Alp, E. E.; Hedman, B.; Hodgson, K. O.; Schoonheydt, R. A.; Sels, B. F.; Solomon, E. I. Structural Characterization of a Non-Heme Iron Active Site in Zeolites That Hydroxylates Methane. *Proc. Natl. Acad. Sci.* **2018**, *115* (18), 4565–4570. https://doi.org/10.1073/pnas.1721717115.

(13) Hammond, C.; Forde, M. M.; Ab Rahim, M. H.; Thetford, A.; He, Q.; Jenkins, R. L.; Dimitratos, N.; Lopez-Sanchez, J. A.; Dummer, N. F.; Murphy, D. M.; Carley, A. F.; Taylor, S. H.; Willock, D. J.; Stangland, E. E.; Kang, J.; Hagen, H.; Kiely, C. J.; Hutchings, G. J. Direct Catalytic Conversion of Methane to Methanol in an Aqueous Medium by Using Copper-Promoted Fe-ZSM-5. *Angew. Chemie Int. Ed.* **2012**, *51* (21), 5129–5133. https://doi.org/10.1002/anie.201108706.

(14) Xiao, D. J.; Bloch, E. D.; Mason, J. A.; Queen, W. L.; Hudson, M. R.; Planas, N.; Borycz, J.; Dzubak, A. L.; Verma, P.; Lee, K.; Bonino, F.; Crocella, V.; Yano, J.; Bordiga, S.; Truhlar, D. G.; Gagliardi, L.; Brown, C. M.; Long, J. R. Oxidation of Ethane to Ethanol by N_2O in a Metal–Organic Framework with Coordinatively Unsaturated Iron(II) Sites. *Nat. Chem.* **2014**, *6* (7), 590–595. https://doi.org/10.1038/nchem.1956.

(15) Verma, P.; Vogiatzis, K. D.; Planas, N.; Borycz, J.; Xiao, D. J.; Long, J. R.; Gagliardi, L.; Truhlar, D. G. Mechanism of Oxidation of Ethane to Ethanol at Iron(IV)–Oxo Sites in Magnesium-Diluted Fe_2(Dobdc). *J. Am. Chem. Soc.* **2015**, *137* (17), 5770–5781. https://doi.org/10.1021/jacs.5b00382.

(16) Kang, Y.-S.; Lu, Y.; Chen, K.; Zhao, Y.; Wang, P.; Sun, W.-Y. Metal–Organic Frameworks with Catalytic Centers: From Synthesis to Catalytic Application. *Coord. Chem. Rev.* **2019**, *378*, 262–280. https://doi.org/10.1016/j.ccr.2018.02.009.

(17) Rogge, S. M. J.; Bavykina, A.; Hajek, J.; Garcia, H.; Olivos-Suarez, A. I.; Sepúlveda-Escribano, A.; Vimont, A.; Clet, G.; Bazin, P.; Kapteijn, F.; Daturi, M.; Ramos-Fernandez, E. V; Llabrés i Xamena, F. X.; Van Speybroeck, V.; Gascon, J. Metal–Organic and Covalent Organic Frameworks as Single-Site Catalysts. *Chem. Soc. Rev.* **2017**, *46* (11), 3134–3184. https://doi.org/10.1039/C7CS00033B.

(18) Howarth, A. J.; Liu, Y.; Li, P.; Li, Z.; Wang, T. C.; Hupp, J. T.; Farha, O. K. Chemical, Thermal and Mechanical Stabilities of Metal–Organic Frameworks. *Nat. Rev. Mater.* **2016**, *1* (3), 15018. https://doi.org/10.1038/natrevmats.2015.18.

(19) Vitillo, J. G.; Bhan, A.; Cramer, C. J.; Lu, C. C.; Gagliardi, L. Quantum Chemical Characterization of Structural Single Fe(II) Sites in MIL-Type Metal-Organic Frameworks for the Oxidation of Methane to Methanol and Ethane to Ethanol. *ACS Catal.* **2019**, *9* (4), 2870–2879. https://doi.org/10.1021/acscatal.8b04813.

(20) Feng, D.; Wang, K.; Wei, Z.; Chen, Y. P.; Simon, C. M.; Arvapally, R. K.; Martin, R. L.; Bosch, M.; Liu, T. F.; Fordham, S.; Yuan, D.; Omary, M. A.; Haranczyk, M.; Smit, B.; Zhou, H. C. Kinetically Tuned Dimensional Augmentation as a Versatile Synthetic Route towards Robust Metal-Organic Frameworks. *Nat. Commun.* **2014**, *5* (1), 5723. https://doi.org/10.1038/ncomms6723.

(21) Simons, M. C.; Vitillo, J. G.; Babucci, M.; Hoffman, A. S.; Boubnov, A.; Beauvais, M. L.; Chen, Z.; Cramer, C. J.; Chapman, K. W.; Bare, S. R.; Gates, B. C.; Lu, C. C.; Gagliardi, L.; Bhan, A. Structure, Dynamics, and Reactivity for Light Alkane Oxidation of Fe(II) Sites Situated in the Nodes of a Metal-Organic Framework. *J. Am. Chem. Soc.* **2019**, *141* (45), 18142–18151. https://doi.org/10.1021/jacs.9b08686.

(22) Rosen, A. S.; Notestein, J. M.; Snurr, R. Q. Identifying Promising Metal–Organic Frameworks for Heterogeneous Catalysis via High-Throughput Periodic Density Functional Theory. *J. Comput. Chem.* **2019**, *40* (12), 1305–1318. https://doi.org/10.1002/jcc.25787.

(23) Rosen, A. S.; Notestein, J. M.; Snurr, R. Q. Structure-Activity Relationships That Identify Metal-Organic Framework Catalysts for Methane Activation. *ACS Catal.* **2019**, *9* (4), 3576–3587. https://doi.org/10.1021/acscatal.8b05178.

(24) Baik, M. H.; Newcomb, M.; Friesner, R. A.; Lippard, S. J. Mechanistic Studies on the Hydroxylation of Methane by Methane Monooxygenase. *Chem. Rev.* **2003**, *103* (6), 2385–2419. https://doi.org/10.1021/cr950244f.

(25) He, X.; Ortiz De Montellano, P. R. Radical Rebound Mechanism in Cytochrome P-450-Catalyzed Hydroxylation of the Multifaceted Radical Clocks Alpha- and Beta-Thujone. *J. Biol. Chem.* **2004**, *279* (38), 39479–39484. https://doi.org/10.1074/jbc.M406838200.

(26) Krebs, C.; Galonić Fujimori, D.; Walsh, C. T.; Bollinger, J. M. Non-Heme Fe(IV)–Oxo Intermediates. *Acc. Chem. Res.* **2007**, *40* (7), 484–492. https://doi.org/10.1021/ar700066p.

(27) Hall, J. N.; Bollini, P. Low-Temperature, Ambient Pressure Oxidation of Methane to Methanol Over Every Tri-Iron Node in a Metal–Organic Framework Material. *Chem. - A Eur. J.* **2020**, *26* (70), 16639–16643. https://doi.org/10.1002/chem.202003894.

(28) Nechita, M. T.; Berlier, G.; Ricchiardi, G.; Bordiga, S.; Zecchina, A. New Precursor for the Post-Synthesis Preparation of Fe-ZSM-5 Zeolites with Low Iron Content. *Catal. Letters* **2005**, *103* (1–2), 33–41. https://doi.org/10.1007/s10562-005-6500-z.

(29) Vitillo, J. G.; Gagliardi, L. Thermal Treatment Effect on CO and NO Adsorption on Fe(II) and Fe(III) Species in Fe 3 O-Based MIL-Type Metal–Organic Frameworks: A Density Functional Theory Study. *Inorg. Chem.* **2021**, In Press. https://doi.org/10.1021/acs.inorgchem.1c01044.

(30) Wilke, M.; Farges, F.; Petit, P. E.; Brown, G. E.; Martin, F. Oxidation State and Coordination of Fe in Minerals: An Fe K-XANES Spectroscopic Study. *Am. Mineral.* **2001**, *86* (5–6), 714–730. https://doi.org/10.2138/am-2001-5-612.

(31) Boubnov, A.; Lichtenberg, H.; Mangold, S.; Grunwaldt, J.-D. Identification of the Iron Oxidation State and Coordination Geometry in Iron Oxide- and Zeolite-Based Catalysts Using Pre-Edge XAS Analysis. *J. Synchrotron Radiat.* **2015**, *22* (2), 410–426. https://doi.org/10.1107/S1600577514025880.

(32) Westre, T. E.; Kennepohl, P.; DeWitt, J. G.; Hedman, B.; Hodgson, K. O.; Solomon, E. I. A Multiplet Analysis of Fe K-Edge 1s → 3d Pre-Edge Features of Iron Complexes. *J. Am. Chem. Soc.* **1997**, *119* (27), 6297–6314. https://doi.org/10.1021/JA964352A.

(33) Starokon, E. V.; Parfenov, M. V.; Pirutko, L. V.; Abornev, S. I.; Panov, G. I. Room-Temperature Oxidation of Methane by α-Oxygen and Extraction of Products from the FeZSM-5 Surface. *J. Phys. Chem. C* **2011**, *115* (5), 2155–2161. https://doi.org/10.1021/jp109906j.

(34) Wood, B. R.; Reimer, J. A.; Bell, A. T.; Janicke, M. T.; Ott, K. C. Methanol Formation on Fe/Al-MFI via the Oxidation of Methane by Nitrous Oxide. *J. Catal.* **2004**, *225* (2), 300–306. https://doi.org/10.1016/j.jcat.2004.04.010.

(35) Leclerc, H.; Vimont, A.; Lavalley, J.-C.; Daturi, M.; Wiersum, A. D.; Llwellyn, P. L.; Horcajada, P.; Férey, G.; Serre, C. Infrared Study of the Influence of Reducible Iron(III) Metal Sites on the Adsorption of CO, CO_2, Propane, Propene and Propyne in the Mesoporous Metal–Organic Framework MIL-100. *Phys. Chem. Chem. Phys.* **2011**, *13* (24), 11748. https://doi.org/10.1039/c1cp20502a.

(36) Yoon, J. W.; Seo, Y. K.; Hwang, Y. K.; Chang, J. S.; Leclerc, H.; Wuttke, S.; Bazin, P.; Vimont, A.; Daturi, M.; Bloch, E.; Llewellyn, P. L.; Serre, C.; Horcajada, P.; Grenèche, J. M.; Rodrigues, A. E.; Férey, G. Controlled Reducibility of a Metal-Organic Framework with Coordinatively Unsaturated Sites for Preferential Gas Sorption. *Angew. Chemie - Int. Ed.* **2010**, *49* (34), 5949–5952. https://doi.org/10.1002/anie.201001230.

(37) Moruzzi, G. Theoretical Aspects. In *Microwave, Infrared, and Laser Transitions of Methanol Atlas of Assigned Lines from 0 to 1258 cm-1*; CRC Press: Boca Raton, 1995; pp 8–9. https://doi.org/10.1201/9781351074650.

(38) Vitillo, J. G.; Lu, C. C.; Cramer, C. J.; Bhan, A.; Gagliardi, L. Influence of First and Second Coordination Environment on Structural Fe(II) Sites in MIL-101 for C−H Bond Activation in Methane. *ACS Catal.* **2021**, *11* (2), 579–589. https://doi.org/10.1021/acscatal.0c03906.

(39) Yang, D.; Bernales, V.; Islamoglu, T.; Farha, O. K.; Hupp, J. T.; Cramer, C. J.; Gagliardi, L.; Gates, B. C. Tuning the Surface Chemistry of Metal Organic Framework Nodes: Proton Topology of the Metal-Oxide-Like Zr_6 Nodes of UiO-66 and NU-1000. *J. Am. Chem. Soc.* **2016**, *138* (46), 15189–15196. https://doi.org/10.1021/jacs.6b08273.

(40) Alecu, I. M.; Zheng, J.; Zhao, Y.; Truhlar, D. G. Computational Thermochemistry: Scale Factor Databases and Scale Factors for Vibrational Frequencies Obtained from Electronic Model Chemistries. *J. Chem. Theory Comput.* **2010**, *6* (9), 2872–2887. https://doi.org/10.1021/ct100326h.

(41) Alayon, E. M. C.; Nachtegaal, M.; Ranocchiari, M.; van Bokhoven, J. A. Catalytic Conversion of Methane to Methanol over Cu–Mordenite. *Chem. Commun.* **2012**, *48* (3), 404–406. https://doi.org/10.1039/C1CC15840F.

(42) Moses, P. G.; Nørskov, J. K. Methanol to Dimethyl Ether over ZSM-22: A Periodic Density Functional Theory Study. *ACS Catal.* **2013**, *3* (4), 735–745. https://doi.org/10.1021/cs300722w.

(43) Sun, J.; Yang, G.; Yoneyama, Y.; Tsubaki, N. Catalysis Chemistry of Dimethyl Ether Synthesis. *ACS Catal.* **2014**, *4* (10), 3346–3356. https://doi.org/10.1021/cs500967j.

(44) Sierraalta, A.; Añez, R.; Coll, D. S.; Alejos, P. Conversion of Methanol to Dimethyl Ether over Silicoaluminophosphates: Isolated Acid Sites and the Influence of Silicon Islands. A DFT-ONIOM Study. *Microporous Mesoporous Mater.* **2020**, *292*, 109732. https://doi.org/10.1016/j.micromeso.2019.109732.

(45) Jones, A. J.; Iglesia, E. Kinetic, Spectroscopic, and Theoretical Assessment of Associative and Dissociative Methanol

Dehydration Routes in Zeolites. *Angew. Chemie - Int. Ed.* **2014**, *53* (45), 12177–12181. https://doi.org/10.1002/anie.201406823.

(46) Janik, M. J.; Macht, J.; Iglesia, E.; Neurock, M. Correlating Acid Properties and Catalytic Function: A First-Principles Analysis of Alcohol Dehydration Pathways on Polyoxometalates. *J. Phys. Chem. C* **2009**, *113* (5), 1872–1885. https://doi.org/10.1021/jp8078748.

(47) Cho, K.-B.; Hirao, H.; Shaik, S.; Nam, W. To Rebound or Dissociate? This Is the Mechanistic Question in C–H Hydroxylation by Heme and Nonheme Metal–Oxo Complexes. *Chem. Soc. Reivews* **2016**, *45* (5), 1197–1210. https://doi.org/10.1039/C5CS00566C.

Table of Contents (TOC) graphic